PAPER

Pressure-induced phase transition of La$_2$Zr$_2$O$_7$ and La$_{0.5}$Gd$_{1.5}$Zr$_2$O$_7$ pyrochlore†

Jingjing Niu, [ID] *[ac] Xiang Wu,[b] Haibin Zhang [ID][c] and Shan Qin[a]

In situ high-pressure experiments on La$_2$Zr$_2$O$_7$ and La$_{0.5}$Gd$_{1.5}$Zr$_2$O$_7$ have been carried out at up to approximately 40 GPa using synchrotron X-ray diffraction and Raman spectroscopy combined with a diamond anvil cell technique. Both La$_2$Zr$_2$O$_7$ and La$_{0.5}$Gd$_{1.5}$Zr$_2$O$_7$ undergo a phase transition from a pyrochlore phase (*Fd$\bar{3}$m*) into a cotunnite-like phase (*Pnma*) at 22.7 and 23.3 GPa, respectively. This type of phase transition is mainly controlled through the order–disorder occupancy of cations, and Gd^{3+} substitution of La^{3+} reduces the stability of zirconate pyrochlore. However, abnormal changes to the unit-cell volumes and vibrational modes observed at 5.5 GPa in La$_2$Zr$_2$O$_7$ and 6.5 GPa in La$_{0.5}$Gd$_{1.5}$Zr$_2$O$_7$ are attributed to an anion disorder in the pyrochlore.

1. Introduction

Rare-earth pyrochlore oxides have been extensively studied and widely applied in many different areas, such as catalysis,[1–3] fuel cells,[4,5] thermal-barrier coatings,[6,7] spin liquids,[8] and the encapsulation of actinide-rich nuclear waste,[9] owing to their various physical and chemical properties. The pyrochlore structure (A$_2$B$_2$O$_6$O′ or A$_2$B$_2$O$_7$), which belongs to *Fd$\bar{3}$m* and Z = 8, can be viewed as A and B cations in an ordered 2 × 2 × 2 fluorite (*Fm$\bar{3}$m* and Z = 2) superlattice structure, with a 1/8 anion deficiency. The pyrochlore structure can be described with different selections of origin. In this paper, the larger A cations occupy 16d (1/2 1/2 1/2) with eight coordinates located in a distorted cubic polyhedron. The six-coordinate B site located at 16c (0 0 0) is usually occupied by smaller cations centered in an oxygen octahedron. The oxygen O^{2-} anions occupy the 48f (x 1/8 1/8) site, whereas the O′$^{2-}$ anions occupy the 8b (3/8 3/8 3/8) site, and the 8a site is systematically vacant.[10] A pyrochlore oxide structure can be viewed as two interpenetrating networks: the first is a corner-shared [BO$_6$] octahedron network and the second is an A$_2$O network similar to an anti cristobalite Cu$_2$O network (Fig. 1a).

An empirical rule demonstrating that, under ambient conditions, A$_2$B$_2$O$_7$ will crystallize into a pyrochlore structure when the average cationic radii ratio r_A/r_B satisfies 1.46 < r_A/r_B <

1.80,[11] which indicates the structural flexibility and composition variety of pyrochlore oxides. If r_A/r_B < 1.46, which indicates that the difference in radii of A^{3+} and B^{4+} is small, A$_2$B$_2$O$_7$ crystallizes in a defected fluorite structure (*Fm$\bar{3}$m*). Otherwise, when r_A/r_B > 1.80, a monoclinic perovskite-like structure (*P2$_1$*) will have more stability under ambient conditions.

In addition to crystallography and other basic studies, the high-pressure behavior of pyrochlore oxides is important to the immobilization of toxic radioactive waste. In the safe immobilization of high-level waste (HLW), toxic actinides are substituted into the lattice and isolated from the biosphere for over 10 000 years underground at a depth of ∼1000 m. A collapse, explosion, and geological changes occurring during isolation may create high pressure on the HLW waste forms, which are enclosed in the disposal repository. As an important thermodynamic parameter, the pressure can strongly affect the structures and properties of the materials, indicating that the high-pressure structure and properties of the substituted pyrochlore oxides are important to high-level waste disposal. Zirconate pyrochlore ceramics are of particular interest because they are resistant to radiation-induced amorphization from the damage arising from the decay of the incorporated actinides.[12,13] Theoretical research has revealed that zirconate pyrochlore (B = Zr^{4+}) and titanite pyrochlore (B = Ti^{4+}) oxides will transfer to an orthorhombic cotunnite-like structure under high pressure (Fig. 1b) (*Pnma* space group, Z = 4).[14–16] The transition pressure of most zirconate pyrochlores is 15–25 GPa, whereas that of titanite pyrochlores is mostly over ∼30 GPa. In general, the incorporation of large radius ions may decrease the phase stability under pressure. An actinide substitution will increase the average cationic radius and affect the structure and properties of pyrochlore oxides. So in the present study, we conducted a comparative study of La$_2$Zr$_2$O$_7$ and La$_{0.5}$Gd$_{1.5}$Zr$_2$O$_7$ pyrochlores at up to approximately 40 GPa to explore the

[a]Key Laboratory of Orogenic Belts and Crustal Evolution, School of Earth and Space Sciences, MOE, Peking University, Beijing 100871, P. R. China. E-mail: sessnjj@pku.edu.cn

[b]State Key Laboratory of Geological Processes and Mineral Resources, China University of Geosciences (Wuhan), 430074, P. R. China

[c]Innovation Research Team for Advanced Ceramics, Institute of Nuclear Physics and Chemistry, China Academy of Engineering Physics, Mianyang, 621900, China
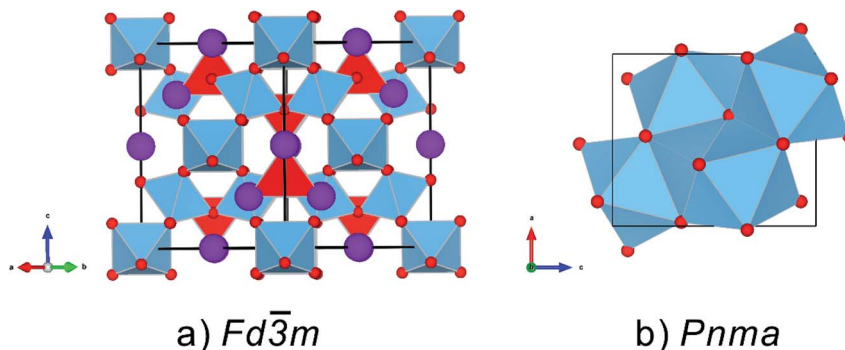
Fig. 1 (a) Crystal structure of $A_2B_2O_7$ pyrochlore oxides, where the purple balls are A^{3+}, the red small balls are O^{2-}, the blue cornered-linked octahedrons are $[BO_6]$, and the red tetrahedrons are $[OA_4]$. (b) Cotunnite-like structure of $A_2B_2O_7$, where the A^{3+} and B^{4+} cations are disordered, and 1/8 of O^{2-} are randomly vacant as compared with the cotunnite structure of AX_2.

influence on the phase stability and compression behavior under a Gd^{3+} substitute. In this manuscript, high pressure phase stability and compression behavior of the two samples are provided. The annealing temperature has an effect on the high-pressure stability and compression behavior,[17,18] and in our study, the sample preparation process is carefully controlled.

2. Experiment details

The sample in the present study was synthesized using a combustion method. The starting materials n-propyl zirconate $[Zr(C_{12}H_{28}O_4)]$ (Aladdin, 70 wt% in n-propanol), $Gd(NO_3)_3 \cdot 6H_2O$ (Aladdin, 99.9%), and $La(NO_3)_3 \cdot 6H_2O$ (Aladdin, 99.9%) were dissolved stoichiometrically in nitric acid and deionized water, respectively, with magnetic stirring. The solutions were mixed together. Glycine (Aladdin, 99%) as a fuel with a mole ratio $n(Gly)/n(Zr) = 2.8$ was added in the mixed solution. This mixture was heated on a hot plate until auto-ignition was reached in a corundum crucible. The solid obtained was annealed at 1773 K for 3 h in an air atmosphere. XRD under ambient conditions using Mo Kα ($\lambda = 0.7093$ Å) confirmed that both samples were in a single pyrochlore phase. The unit cell parameters (a-axial length a) of $La_2Zr_2O_7$ and $La_{0.5}Gd_{1.5}Zr_2O_7$ are 10.7949(3) Å and 10.5762(3) Å, respectively, which are in good agreement with previous reports.[19]

In *in situ* synchrotron X-ray diffraction experiments, symmetry-type diamond anvil cells (DACs) were employed as a high-pressure apparatus. This was carried out by applying a focused monochromatic beam of $\lambda = 0.6199$ Å using a 4W2 beamline at the Beijing Synchrotron Radiation Facility. Rhenium gaskets were pre-indented as sample chambers to ~40 μm in thickness with a hole ~150 μm in diameter at the center of the indentation. The samples were compressed into thin slices using a couple of WC anvils and were loaded into the sample chambers. The pressure transmitting medium (PTM) was silicone oil and the pressure was monitored using the ruby fluorescence method.[20] Uncertainties in pressure are <1 GPa for pressures of below 40 GPa and ~2 GPa for pressures above 40 GPa. All XRD spectra were converted from Debye rings into

one-dimensional X-ray profiles *versus* 2θ using the FIT2D code.[21] The high-pressure XRD patterns were fitted using the Le Bail method implemented with GSAS+EXPGUI software.[22]

An *in situ* high-pressure Raman experiment was carried out at room temperature on a Renishaw inVia reflex laser Raman spectrometer. A 532 nm diode-pumped solid-state laser was employed as the excitation light source. The spectra were calibrated using a silicon wafer, and the scattered light was collected in backscattering geometry using a charge-coupled device detector with a resolution of 1 cm^{-1}. Two samples, $La_2Zr_2O_7$ and $La_{0.5}Gd_{1.5}Zr_2O_7$, were compressed into slices and placed into one single 150 μm diameter hole drilled in pre-indented Rhenium gaskets to avoid differences in the sample loading conditions in the diamond anvil cell. The ruby fluorescence technique was employed to calibrate the pressure.[20] The noble gas argon was used as the pressure transmitting medium (PTM). The Raman spectra were fitted using pseudo-Voigt functions to determine the peak position.

3. Results

The *in situ* high-pressure XRD data of $La_2Zr_2O_7$ and $La_{0.5}Gd_{1.5}$-Zr_2O_7 were collected at up to ~40 GPa, selected XRD patterns of which are shown in Fig. 2. At the beginning of the experiments, all reflections of $La_2Zr_2O_7$ and $La_{0.5}Gd_{1.5}Zr_2O_7$ can be indexed to the $Fd\bar{3}m$ space group. With an increase in pressure, all diffraction peaks shift to a higher 2θ angle owing to the contraction of the lattice. At below ~20 GPa, the Le Bail refinement using the $Fd\bar{3}m$ space group can account for nearly all of the intense reflections observed.

$La_2Zr_2O_7$ and $La_{0.5}Gd_{1.5}Zr_2O_7$ underwent a pressure-induced phase transition at above 22 GPa. The onset of the high-pressure stable phase is identified by a new reflection arising between the (222) and (400) reflections of pyrochlore,[17,23] and the high-pressure phase is a *Pnma* cotunnite-like phase. The onset of the high-pressure phase is approximately equivalent for both $La_2Zr_2O_7$ and $La_{0.5}Gd_{1.5}Zr_2O_7$ (22.7 and 23.3 GPa, respectively). The transition is sluggish and both structures co-exist until reaching the highest pressure. The diffraction data collected
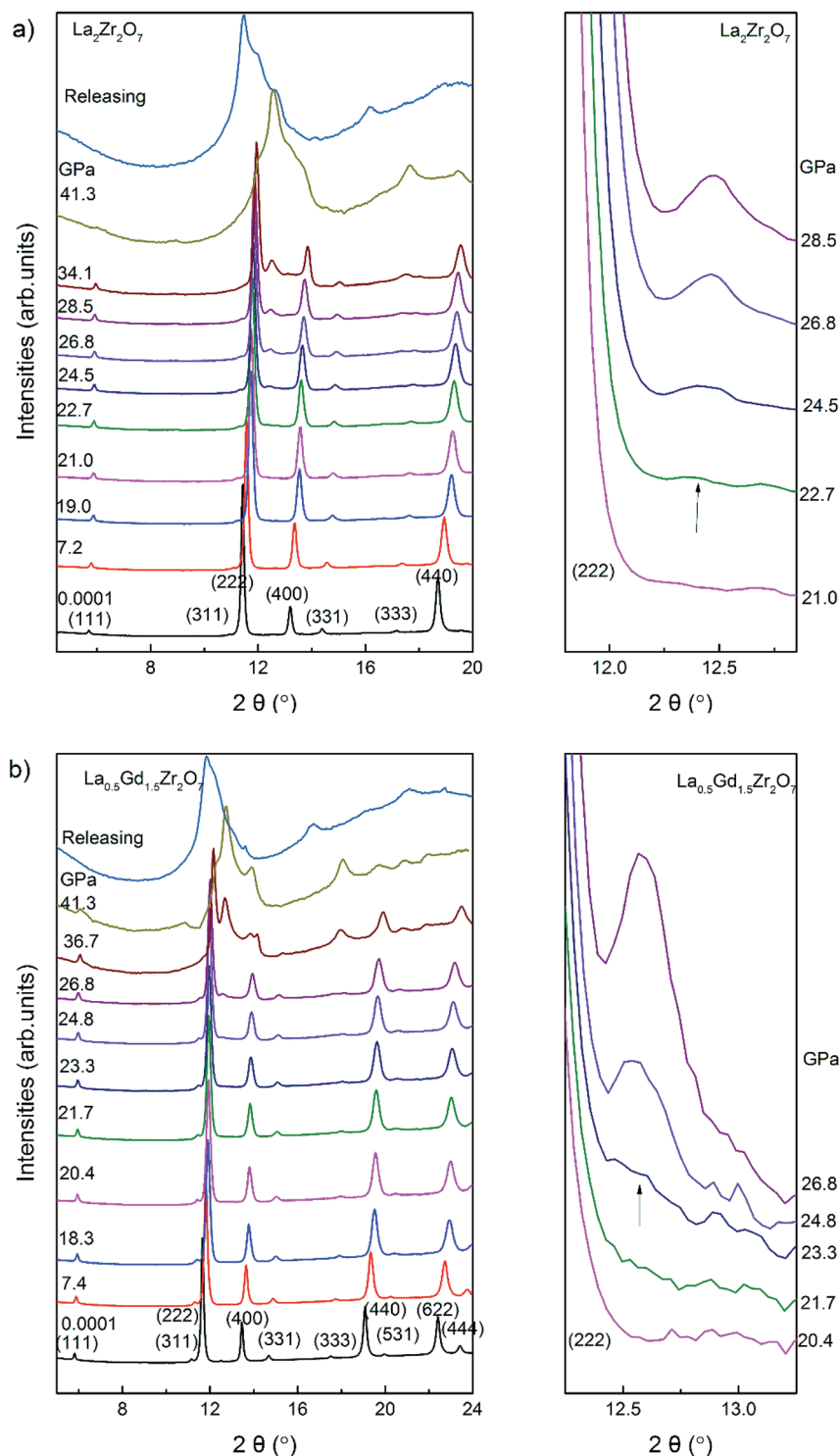
Fig. 2 *In situ* high-pressure XRD pattern of (a) $La_2Zr_2O_7$ and (b) $La_{0.5}Gd_{1.5}Zr_2O_7$. The enlargement of patterns from ~21 to 28 GPa within a 2θ range of 12.4–13.1° shows new reflections arising at 22.7 GPa in $La_2Zr_2O_7$ and at 23.3 GPa in $La_{0.5}Gd_{1.5}Zr_2O_7$, indicating the formation of a high-pressure phase.

upon quenching to the ambient condition are difficult to identify in the phase.

According to group theory, pyrochlore structure oxides have six Raman active modes, namely,

$$\Gamma = A_{1g} + E_g + 4F_{2g} \qquad (1)$$

In situ high-pressure Raman spectra of $La_2Zr_2O_7$ and $La_{0.5}Gd_{1.5}Zr_2O_7$ recorded from 150 to 800 cm^{-1} at various pressures in run 1 are shown in Fig. 3. At the beginning of the experiment,
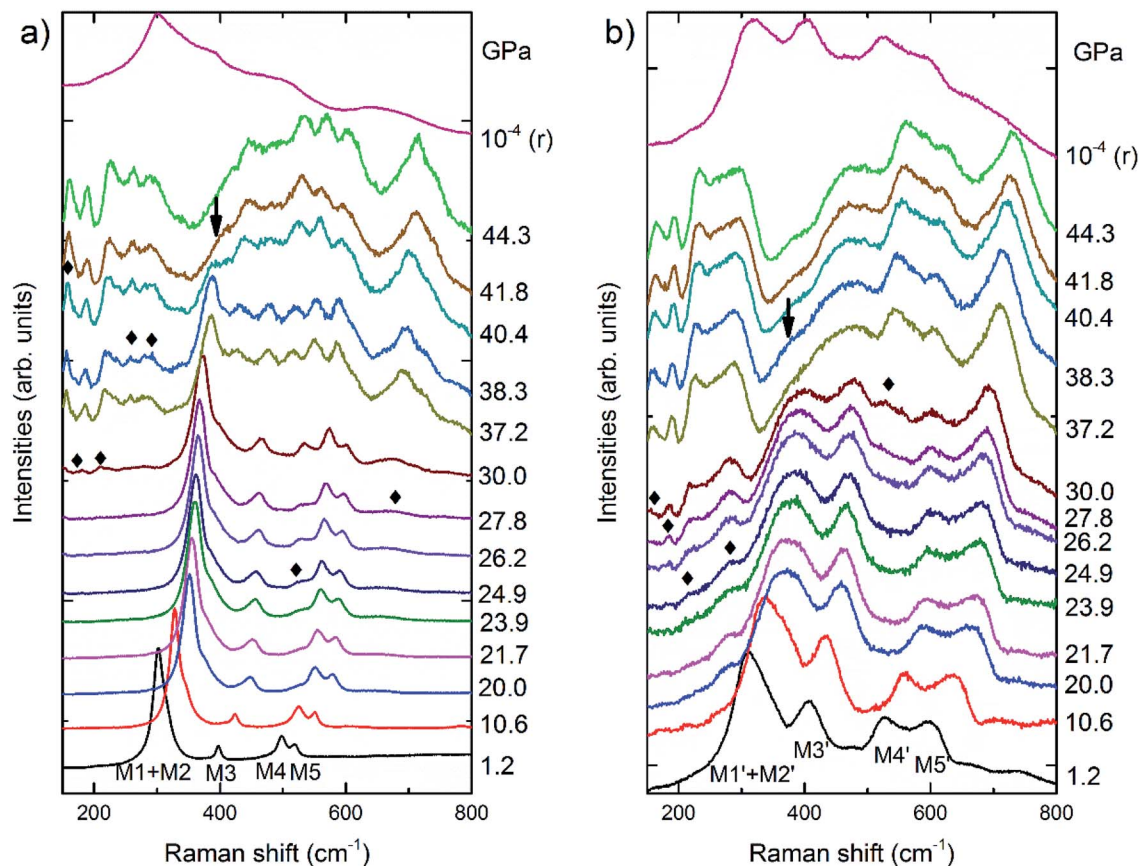
Fig. 3 *In situ* high-pressure Raman spectra in run 1 of (a) $La_2Zr_2O_7$ and (b) $La_{0.5}Gd_{1.5}Zr_2O_7$. The new bands attributed to the high-pressure cotunnite-like phase are marked by black diamonds at the lowest pressure at which they first appear.

comparing with previous studies,[24–26] five Raman modes of the pyrochlore phase can be identified in both $La_2Zr_2O_7$ and $La_{0.5}$-$Gd_{1.5}Zr_2O_7$. In $La_2Zr_2O_7$, the band at ~300 cm^{-1} is made up of two Raman modes: one intense E_g mode associated with O–Zr–O bending in [ZrO_6] octahedrons and demonstrating M1, and a weak F_{2g} mode associated with La–O′ stretching demonstrating M2. M3 at ~380 cm^{-1} is an F_{2g} mode associated with the vibrations of oxygen anions (O–O′), and M4 at ~500 cm^{-1} is another F_{2g} mode and is associated with Zr–O stretching. The band at ~515 cm^{-1} is an A_{1g} mode and is associated with La–O stretching. In $La_{0.5}Gd_{1.5}Zr_2O_7$, M1′ + M2′ are E_g + F_{2g} modes similar to those of $La_2Zr_2O_7$, M3′ at ~400 cm^{-1} and M5′ at ~600 cm^{-1} are two F_{2g} modes associated with Zr–O and R–O stretching vibrations, and M4′ at ~550 cm^{-1} is A_{1g} mode associated with R–O stretching. The Raman spectra of $La_2Zr_2O_7$ have sharper and better-defined peaks than those of $La_{0.5}Gd_{1.5}Zr_2O_7$. All Raman bands shift to higher frequencies with an increase in pressure. At above 24.9 GPa, new Raman bands (marked using the diamonds in Fig. 3a and b) are shown in both $La_2Zr_2O_7$ and $La_{0.5}Gd_{1.5}Zr_2O_7$. These new bands belong to the vibrations from the cotunnite-like phase, and the identified transition induced by the pressure begins at ~24.9 GPa, which is slightly higher than the *in situ* high-pressure XRD results. With a further increase in pressure, the intensity of the M1 peak of both samples decreases. At above 41.8 GPa, the M1 peak in $La_2Zr_2O_7$

disappears, whereas in $La_{0.5}Gd_{1.5}Zr_2O_7$ the peak pressure disappears at 38.3 GPa, which indicates that the transitions are complete. Thus, the pyrochlore-to-cotunnite-like transition ends at 41.8 and 38.3 GPa in $La_2Zr_2O_7$ and $La_{0.5}Gd_{1.5}Zr_2O_7$, respectively. The transition end pressure here is denoted as P_e. The spectrum of $La_2Zr_2O_7$ and $La_{0.5}Gd_{1.5}Zr_2O_7$ recovered from ~44 GPa has a significantly different characteristic from the cotunnite-like phase. A previous study[24] showed that $La_2Zr_2O_7$ will transfer into a defected fluorite structure from a cotunnite-like structure as the pressure is released. The Raman spectrum recovered from the highest pressure in $La_2Zr_2O_7$ shows a mixture of a high-pressure phase and a defected-fluorite phase, and thus the transition in $La_2Zr_2O_7$ is irreversible. However, the spectrum of $La_{0.5}Gd_{1.5}Zr_2O_7$ recovered from the highest pressure is quite similar to the starting pyrochlore structure, which means that $La_{0.5}Gd_{1.5}Zr_2O_7$ will recover to a pyrochlore structure during quenching, which is reversible.

The cell volume obtained through the Le Bail refinement of the XRD patterns as a function of pressure is plotted in Fig. 4. The *P–V* curves of $La_2Zr_2O_7$ and $La_{0.5}Gd_{1.5}Zr_2O_7$ show changes in slope at 5.5 and 6.5 GPa, respectively. The sudden pressure increases in the bulk modulus are indicated by P_c. These *P–V* data are fitted to the Birch–Murnaghan equation of state (EoS)[27] in different pressure regions:
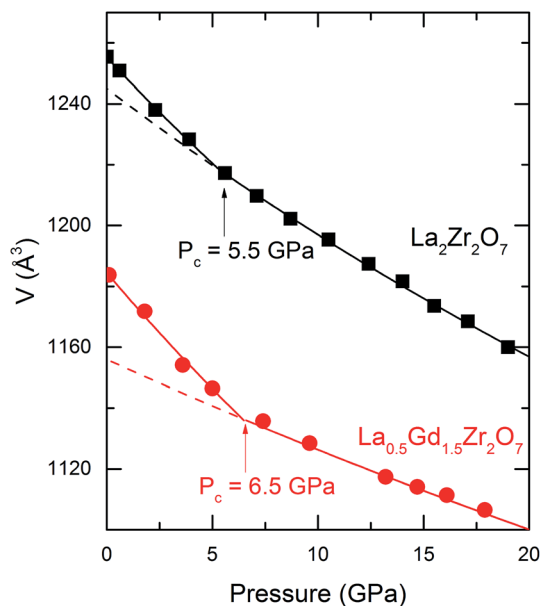
Fig. 4 The volume of $La_2Zr_2O_7$ and $La_{0.5}Gd_{1.5}Zr_2O_7$ as a function of pressure. The black squares and red circles are the unit-cell volumes at different pressures. The black and red solid lines correspond to the B–M EoS fitting for $La_2Zr_2O_7$ and $La_{0.5}Gd_{1.5}Zr_2O_7$, respectively. Changes in the compressibility can be observed in both samples. In $La_2Zr_2O_7$, the changing pressure is 5.5 GPa, and in $La_{0.5}Gd_{1.5}Zr_2O_7$ is 6.5 GPa.

$$P = \frac{3}{2}B_0\left[\left(\frac{V_0}{V}\right)^{\frac{7}{3}} - \left(\frac{V_0}{V}\right)^{\frac{5}{3}}\right] \times \left\{1 + \frac{3}{4}\left(B_0' - 4\right)\left[\left(\frac{V_0}{V}\right)^{\frac{2}{3}} - 1\right]\right\}$$
(2)

where P is the pressure, B_0 is the bulk modulus, B_0' is the pressure derivative of B_0, and V_0 is the unit-cell volume at zero pressure and room temperature. The second-order Birch–Murnaghan P–V EoS ($B_0' = 4$ fixed) was employed to obtain the zero-pressure bulk modulus (B_0) for both $P < P_c$ and $P > P_c$, and P_c is calculated from the intersection of the two P–V curves. The EoS parameters are listed in Table 1. In $La_2Zr_2O_7$, at 5.5 GPa, the bulk modulus increases from 168(3) to 235(4) GPa, and V_0 decreases from 1255.3(3) to 1245(1) Å^3. In $La_{0.5}Gd_{1.5}Zr_2O_7$, when $P < 6.5$ GPa, the bulk modulus is 142.6(9) GPa, which indicates that the Gd^{3+} substitution La^{3+} decreases the bulk modulus and makes the pyrochlore more compressible. When $P > 6.5$ GPa, the bulk modulus increases to 360(23) GPa, which indicates that the $La_{0.5}Gd_{1.5}Zr_2O_7$ becomes strongly incompressible when the pressure is higher than 6.5 GPa. The bulk modulus B_0 of the two

samples before P_c are both about ~160 GPa, which is lower than those of other titanite pyrochlores (e.g. $B_0(Sm_2Ti_2O_7)$ = 185.4(2) GPa, $B_0(Gd_2Ti_2O_7)$ = 176(4) GPa, $B_0(Tb_2Ti_2O_7)$ = 199(1) GPa.),[28–30] for Zr^{4+} owns a lager cationic radius and the bond length of Zr–O is longer than that of Ti–O.

The observed Raman shift frequencies with an increasing pressure of $La_2Zr_2O_7$ and $La_{0.5}Gd_{1.5}Zr_2O_7$ are plotted in Fig. 5. We applied a linear function to fit the Raman frequencies as a function of pressure,

$$\nu = \nu_0 + kP$$
(3)

where ν is the frequency of the Raman mode, ν_0 is the phonon frequency at ambient pressure, P is pressure, and k is the coefficient of P and ν. The Grüneisen parameters are calculated using the linear pressure coefficients of the wavenumber (dν/dp), and the measured bulk modulus (listed in Table 1). The mode Grüneisen parameters γ and the coefficients dν/dp are listed in Table 2. At ~5 GPa, clear changes in slope are observed in all the Raman active modes for $La_2Zr_2O_7$. However, changes in slope are observed only in M1–M4 modes in $La_{0.5}Gd_{1.5}Zr_2O_7$, and P_c is ~6 GPa. No significant changes in slope occur in M5. The changes in slope of the vibration modes in $La_2Zr_2O_7$ and $La_{0.5}Gd_{1.5}Zr_2O_7$ indicate that the incompressibility at P_c is likely due to the intrinsic property of the samples.

4. Discussion

4.1 Transition pressure

The pressures at which the cotunnite-like phase first appears (P_s) and where the high-pressure phase occupies the entire volume of the same (P_e) are listed in Table 3. $La_2Zr_2O_7$ began to transfer to the cotunnite-like structure at 22.7 GPa, and the transition complete at 41.8 GPa. While the starting pressure of the transition of $La_{0.5}Gd_{1.5}Zr_2O_7$ is 23.3, but the transition finishes at 38.7 GPa. The pressure-induced transition from the pyrochlore phase to the cotunnite-like phase is sluggish, and both structures co-exist over a pressure range of approximately 20 GPa. The theoretical calculation predicts that a smaller radius of the A-site cation may lower the transition.[16] Here, P_s appears to be constant as a function of the cationic radius ratio. This may be explained based on differences in the sample loading conditions in a diamond anvil cell and/or by a slight overshoot at the onset of the transition when increasing the pressure during the experiment. Here, P_e of $La_2Zr_2O_7$ is ~4 GPa higher than that of $La_{0.5}Gd_{1.5}Zr_2O_7$. This reveals a tendency that P_e decreases when a decrease in the ionic radius of the A-site

Table 1 The unit cell volume and bulk modulus at zero pressure (V_0, B_0) of B–M EoS obtained from *in situ* high-pressure synchrotron XRD experiments

	$P < P_c$			$P > P_c$		
	V_0 (Å^3)	B_0 (GPa)	B_0'	V_0 (Å^3)	B_0 (GPa)	B_0'
$La_2Zr_2O_7$	1255.3 (3)	168 (3)	4 (fixed)	1245 (1)	235 (4)	4 (fixed)
$La_{0.5}Gd_{1.5}Zr_2O_7$	1184.6 (2)	142.6 (9)		1156 (2)	360 (23)	
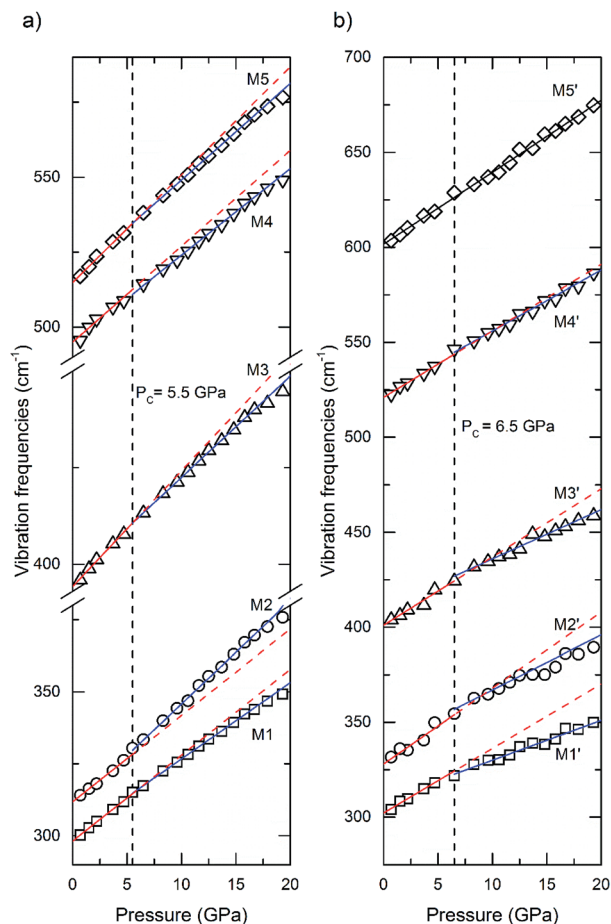
Fig. 5 Pressure dependence of Raman modes for (a) $La_2Zr_2O_7$ and (b) $La_{0.5}Gd_{1.5}Zr_2O_7$. The solid lines are the linear function of the vibration frequencies and pressure. The red lines indicate the region below P_c and the blue lines show the region above P_c.

cations r_A. This is consistent with the Surblé et al.'s high-pressure study on $Ln_2Zr_2O_7$ pyrochlore (Ln = Ce, Nd, Gd),[31] and it has also been predicted that the P_e of $La_2Zr_2O_7$ is 43 ± 2 GPa, which was confirmed by our results. Usually, the

incorporation of a larger radius cation will decrease the transition pressure, e.g. the olivine–spinel transition pressure of Mg_2SiO_4 (12.5 GPa) and Fe_2SiO_4 (4.9 GPa).[32] However, according to the previous studies,[33] the pressure-induced transition from a pyrochlore structure to a cotunnite-like structure is mainly an order-disorder transition. A phase stability study on $Gd_2Ti_{2-x}Zr_xO_7$ pyrochlore has revealed that the transition pressure is positively related to the cationic radius ratio, and the transition is mainly achieved through a cation exchange at A–B position.[34] All rare-earth elements have a similar crystal chemistry property. The Gd^{3+} substitution in La^{3+} can decrease the average cationic radius of the A-site and lower the differences in the A and B-site cations, making the transition easier. Thus, a smaller cation substitution may lower the transition pressure in the pyrochlore oxides, and decrease the phase stability under pressure. Vice versa, larger radius cation substitution will improve the phase stability under pressure. It indicates that in the immobilization forms of HLW, A-site substitution of actinides will not decrease the transition pressure for their cationic radius are larger than Gd^{3+} or other REE cations.

The value of P_s for the two samples in the present study is ~23 GPa, which is higher than that in a previous experimental study[24] and in other zirconate pyrochlores. In both the present study and Zhang's research,[24] silicone oil was employed as the pressure media during an in situ high pressure XRD, and thus the PTM effect can be excluded. The difference in the transition pressure may be related to the sample preparation. There are two main differences that we believe can increase the pyrochlore phase stability under pressure: first, our samples used in this study were synthesized through a combustion method, whereas others have been synthesized using a solid-state method (similar to $Eu_2Zr_2O_7$ (ref. 25) or $Sm_2Zr_2O_7$ (ref. 35)) or an aqueous route ($Nd_2Zr_2O_7$ or $Gd_2Zr_2O_7$),[31] and the grain size and morphology of the samples from a combustion method are quite different from those of a solid-state method. Second, the annealing temperature in our sample is higher than that in other studies. Rittman et al.'s experimental study[17] proved that a higher annealing temperature can significantly reduce the

Table 2 Experimental pressure coefficients and Grüneisen parameters of $La_2Zr_2O_7$ and $La_{0.5}Gd_{1.5}Zr_2O_7$ at different pressure regions

	$P < P_c$			$P > P_c$		
	$d\nu/dp$ (cm^{-1}/GPa)	γ_i	ν_0 (cm^{-1})	$d\nu/dp$ (cm^{-1}/GPa)	γ_i	ν_0 (cm^{-1})
$La_2Zr_2O_7$						
M1	3.0 (1)	1.69	298.2 (3)	2.65 (3)	1.48	300.2 (3)
M2	3.00 (9)	1.62	311.8 (3)	3.58 (6)	1.94	310.0 (7)
M3	3.0 (1)	1.27	394.2 (4)	2.62 (2)	1.11	396.3 (3)
M4	3.2 (3)	1.08	495 (1)	2.89 (4)	0.98	495.1 (5)
M5	3.6 (2)	1.17	514.8 (5)	3.22 (3)	1.05	516.9 (4)
$La_{0.5}Gd_{1.5}Zr_2O_7$						
M1′	3.4 (2)	1.89	302.2 (6)	2.1 (2)	1.14	309 (3)
M2′	4.0 (8)	2.05	328 (2)	2.9 (3)	1.44	338 (2)
M3′	3.6 (6)	1.51	401 (2)	2.6 (1)	1.07	410 (2)
M4′	3.5 (2)	1.12	521 (5)	3.2 (1)	1.02	524 (2)
M5′	3.79 (6)	1.05	601.6 (7)	—	—	—

Table 3 High-pressure structural stability of $La_2Zr_2O_7$ and $La_{0.5}$-$Gd_{1.5}Zr_2O_7$. The a-axial length a_0 is obtained from the XRD under ambient conditions

Compounds	a_0 (Å)	r_A/r_B	P_s (GPa)	P_e (GPa)
$La_2Zr_2O_7$	10.7949 (3)	1.61	22.7	41.8
$La_{0.5}Gd_{1.5}Zr_2O_7$	10.5762 (3)	1.50	23.3	38.7

concentration of defects in the lattice, and increase the transition pressure P_s. Usually, a combustion method requires a lower annealing temperature (1500 K, 2–3 h)[19] compared with a solid-state method (1800 K, 10 h).[36] In our study, the samples were annealed at 1773 K for 3 h, which is higher than the other combustion path synthesized samples. Considering the two points above, the differences in the sample preparation reduce the defects in the lattices in our samples and increase the phase stabilities. This conclusion indicates that reducing the defect concentrations in the lattice by improving the preparation technology or growth of single crystals will be helpful to improve the HLW forms' phase stability.

4.2 Mechanism of abnormal compressibility changes

In the present study, the changing pressure (P_c) of the compressibility and the pressure dependence of the vibration modes are 5.5 and 6.5 GPa in $La_2Zr_2O_7$ and $La_{0.5}Gd_{1.5}Zr_2O_7$, respectively. Le Bail refinements in the *in situ* synchrotron high-pressure XRD patterns also confirm that the pyrochlore structure remains stable above P_c (Fig. S1†). An anomalous lattice expansion and change in the pressure dependence of the vibration modes were observed in $La_2Zr_2O_7$ at ∼10 GPa, as reported by Zhang *et al.*, and the mechanism is considered to be related to the water from the PTM intercalation.[24] But in the present study, regardless of the silicone oil used in the XRD analysis and the argon shown in the Raman spectra, the PTMs are hydrophobic, water can be excluded in our study, and the incorporation of water in pyrochlore has difficulty explaining the increase in bulk modulus. Cation disorder can be excluded because the intensities of all XRD reflections, particularly the supper lattice reflections (111), (311), (333), and (531) remain constant, which implies that disorder in a cation is rare.

We guess that the abnormal compressibility changes in $La_2Zr_2O_7$ and $La_{0.5}Gd_{1.5}Zr_2O_7$ may be related to the anion distortion. A compressibility change under pressure has been observed in many titanite pyrochlores (such as $Gd_2Ti_2O_7$ (ref. 29) and $Tb_2Ti_2O_7$ (ref. 30)), and is related to the rearrangement of [TiO_6] octahedra. In zirconate pyrochlore, an increase of B_0 have been observed in $Sm_2Zr_2O_7$, and it is thought to be caused by a structural distortion.[35] So the increase of B_0 in $La_2Zr_2O_7$ and $La_{0.5}Gd_{1.5}Zr_2O_7$ may undergo the same mechanism with other pyrochlores. Another possible mechanism is anion disorder, but the XRD is more focused on a long-range structure, whereas an anion disorder is more likely a change in the arrangement of short-range ions. XAFS and PDF, which are more powerful for sensing short-range arrangements, may be helpful in revealing more details on the structural distortion and provide firmer evidence regarding the mechanism of the compression behavior of the pyrochlore oxides.

Re-thinking of the compressibility results reported by previous literature, the B'_0 of $Gd_2Zr_2O_7$, $Nd_2Zr_2O_7$, and $Ce_2Zr_2O_7$ provided in the literature are 8(1), 14(1) and 0.0, which is far from 4.0. These physics violation results indicate that there may be compressibility changes have not been discovered.

4.3 Thermodynamic mechanism of the coexistence of the two phases

In the following, we derive a model from the perspective of thermodynamics to describe the phase ratio of the high-pressure cotunnite-like phase and the pyrochlore phase. The pressure-induced phase transition from a pyrochlore into a cotunnite-like phase can be seen as the following reaction:

$$A_2B_2O_7 \text{ (pyrochlore)} \rightarrow A_2B_2O_7 \text{ (cotunnite-like)}$$
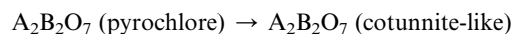
Thus, the chemical equilibrium constant K of the transition can be written as

$$K = \frac{[Cot]}{[Pyro]} \tag{4}$$

where [Cot] is the concentration of the high-pressure phase, and [Pyro] is the concentration of the pyrochlore phase. The temperature used in the present study was constantly set to room temperature. Combining the first and second laws of thermodynamics, the change in Gibbs free energy during the transition can be written as

$$\delta\Delta G = \Delta V dP \tag{5}$$

where ΔV is the volume change in the transition. Here, we assume that ΔV is constant under pressure. We then have

$$-RT d \ln K = \Delta V dP \tag{6}$$

Setting $P_{1/2}$ as the pressure under which the concentration of the high-pressure phase is equal to the pyrochlore phase, we have $P = P_{1/2}$, $K = 1$. Solving the function, we obtain

$$\ln \frac{[Cot]}{[Pyro]} = \frac{-\Delta V}{RT}\left(P_{\frac{1}{2}} - P\right) \tag{7}$$

Although owing to the poor quality of the *in situ* high-pressure XRD patterns and the limit to the X-ray wavelength, obtaining the phase ratio from reliable Rietveld refinements is quite difficult. In previous studies, the increase in the scattering intensity between the (222) and (400) pyrochlore structures has been used to define the onset of the transition because this is the most intense of the cotunnite peaks.[17,23] Here, we use the intensity ratio I/I_{222} between the intensities of the most intense peak of the cotunnite phase and the (222) peak of the pyrochlore to describe the phase ratio of the high-pressure phase and
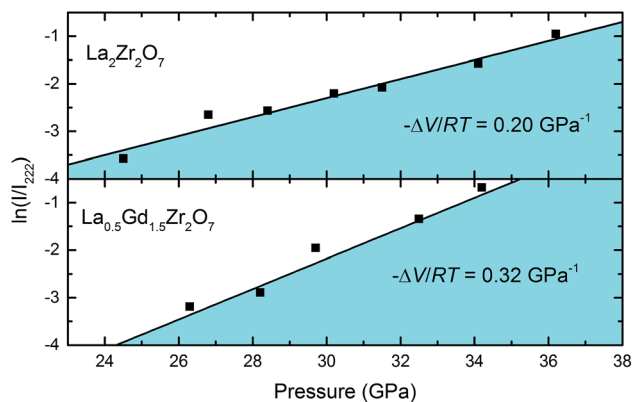
Fig. 6 $\ln(I/I_{222})$ of $La_2Zr_2O_7$ and $La_{0.5}Gd_{1.5}Zr_2O_7$ as functions of pressure.

pyrochlore phase. Clearly, I/I_{222} is proportional to the phase ratio $\dfrac{I}{I_{222}} = \dfrac{1}{q} \dfrac{[\text{Cot}]}{[\text{Pyro}]}$, where q is the coefficient. We then have

$$\ln \frac{I}{I_{222}} = \frac{-\Delta V}{RT}\left(P_{\frac{1}{2}} - P\right) + \ln q \tag{8}$$

Fig. 6 shows $\ln I/I_{222}$ of $La_2Zr_2O_7$ and $La_{0.5}Gd_{1.5}Zr_2O_7$ at various pressures. From the equation, it can be seen that the slope of $\ln I/I_{222}$ with pressure is determined by the volume change in the transition. Liner fits yield a slope of $\ln I/I_{222}$ with a pressure of 0.20 GPa^{-1}, which is lower than that of $La_{0.5}$-$Gd_{1.5}Zr_2O_7$ 0.32 GPa^{-1}. This indicates that the ΔV of $La_2Zr_2O_7$ is smaller during the transition. Theoretical calculations have proven that, during the transition, the ΔV of $La_2Zr_2O_7$ is 9.9% V_0,[16] whereas an experimental study has shown that the ΔV of $Gd_2Zr_2O_7$ is 16.4%V_0,[37] which is in agreement with our prediction. In addition, the volume changes ΔV during the transition also determine the co-existence of two-phase pressure regions. A larger ΔV means a high-pressure phase generates "faster" under pressure, shortening the co-existing region.

5. Conclusion

The high-pressure phase stability of $La_2Zr_2O_7$ and $La_{0.5}Gd_{1.5}$-Zr_2O_7 pyrochlore were examined using synchrotron radiation X-ray diffraction and Raman spectroscopy. Both samples underwent a pressure-induced structural transition leading to a *Pnma* cotunnite-like phase. The P_e of $La_{0.5}Gd_{1.5}Zr_2O_7$ was shown to be lower than that of $La_2Zr_2O_7$, indicating that the transition pressure has a positive correlation with the cationic radius ratio r_A/r_B. The compression behavior of the pyrochlore phase of the two samples was determined. The *P–V* curves reveal that, at over pressure P_c, $La_2Zr_2O_7$ and $La_{0.5}Gd_{1.5}Zr_2O_7$ both show an increase in the bulk modulus, which may be related to the structural distortion under pressure.

Conflicts of interest

There are no conflicts to declare.

References

1 Q. Feng, Q. Wang, Z. Zhang, Y. Y. H. Xiong, H. Y. Li, Y. Yao, X. Z. Yuan, M. C. Williams, M. Gu, H. Chen, H. Li and H. J. Wang, *Appl. Catal., B*, 2019, **244**, 494–501.

2 L. J. Ai, Z. P. Wang, Y. B. Gao, C. C. Cui, B. Q. Wang, W. Liu and L. G. Wang, *J. Mater. Sci.*, 2019, **54**, 4495–4510.

3 J. Zhang, D. Wang, L. Lai, X. Fang, J. Xu, X. Xu, X. Zhang, J. Liu, H. Peng and X. Wang, *Catal. Today*, 2019, **327**, 168–176.

4 B. J. Wuensch, K. W. Eberman, C. Heremans, E. M. Ku, P. Onnerud, E. M. E. Yeo, S. M. Haile, J. K. Stalick and J. D. Jorgensen, *Solid State Ionics*, 2000, **129**, 111–133.

5 K. W. Eberman, B. J. Wuensch and J. D. Jorgensen, *Solid State Ionics*, 2002, **148**, 521–526.

6 N. P. Padture, M. Gell and E. H. Jordan, *Science*, 2002, **296**, 280–284.

7 J. Wu, X. Wei, N. P. Padture, P. G. Klemens, M. Gell, E. García, P. Miranzo and M. I. Osendi, *J. Am. Ceram. Soc.*, 2002, **85**, 3031–3035.

8 M. Gingras, B. Den Hertog, M. Faucher, J. Gardner, S. Dunsiger, L. Chang, B. Gaulin, N. Raju and J. Greedan, *Phys. Rev. B: Condens. Matter Mater. Phys.*, 2000, **62**, 6496.

9 R. C. Ewing, W. J. Weber and J. Lian, *J. Appl. Phys.*, 2004, **95**, 5949–5971.

10 J. S. Gardner, M. J. Gingras and J. E. Greedan, *Rev. Mod. Phys.*, 2010, **82**, 53.

11 M. Subramanian, G. Aravamudan and G. S. Rao, *Prog. Solid State Chem.*, 1983, **15**, 55–143.

12 K. E. Sickafus, L. Minervini, R. W. Grimes, J. A. Valdez, M. Ishimaru, F. Li, K. J. Mcclellan and T. Hartmann, *Science*, 2000, **289**, 748–751.

13 R. C. Ewing, W. J. Weber and F. W. C. Jr, *Prog. Nucl. Energy*, 1995, **29**, 63–127.

14 H. Y. Xiao, F. Gao and W. J. Weber, *Phys. Rev. B: Condens. Matter Mater. Phys.*, 2009, **80**, 212102.

15 H. Y. Xiao and W. J. Weber, *J. Phys.: Condens. Matter*, 2011, **23**, 035501.

16 H. Y. Xiao, F. Zhang, F. Gao, M. Lang, R. C. Ewing and W. J. Weber, *Phys. Chem. Chem. Phys.*, 2010, **12**, 12472–12477.

17 D. R. Rittman, K. M. Turner, S. Park, A. F. Fuentes, C. Park, R. C. Ewing and W. L. Mao, *Sci. Rep.*, 2017, **7**, 2236.

18 F. Zhang, M. Lang and R. Ewing, *Appl. Phys. Lett.*, 2015, **106**, 191902.

19 K. A. Sakharov, E. P. Simonenko, N. P. Simonenko, M. L. Vaganova, Y. E. Lebedeva, A. S. Chaynikova,

I. V. Osin, O. Y. Sorokin, D. V. Grashchenkov and V. G. Sevastyanov, *Ceram. Int.*, 2018, **44**, 7647–7655.

20 H. Mao, J.-A. Xu and P. Bell, *J. Geophys. Res.: Solid Earth*, 1986, **91**, 4673–4676.

21 A. Hammersley, S. Svensson, M. Hanfland, A. Fitch and D. Hausermann, *High Pressure Res.*, 1996, **14**, 235–248.

22 B. H. Toby, *J. Appl. Crystallogr.*, 2001, **34**, 210–213.

23 D. R. Rittman, K. M. Turner, S. Park, A. F. Fuentes, J. Yan, R. C. Ewing and W. L. Mao, *J. Appl. Phys.*, 2017, **121**, 045902.

24 F. Zhang, M. Lang, Z. Liu and R. Ewing, *Phys. Rev. Lett.*, 2010, **105**, 015503.

25 H. Li, N. Li, Y. Li, Q. Tao, Y. Zhao, H. Zhu, Y. Ma, P. Zhu and X. Wang, *High Pressure Res.*, 2017, **37**, 256–266.

26 X. L. Xia, Z. G. Liu, J. H. Ouyang and Y. Zheng, *Fuel Cells*, 2012, **12**, 624–632.

27 F. Birch, *Phys. Rev.*, 1947, **71**, 809.

28 B. Winkler, A. Friedrich, W. Morgenroth, E. Haussühl, V. Milman, C. R. Stanek and K. J. McClellan, *Chin. Sci. Bull.*, 2014, **59**, 5278–5282.

29 S. Saha, D. Muthu, C. Pascanut, N. Dragoe, R. Suryanarayanan, G. Dhalenne, A. Revcolevschi, S. Karmakar, S. M. Sharma and A. Sood, *Phys. Rev. B: Condens. Matter Mater. Phys.*, 2006, **74**, 064109.

30 S. Saha, D. S. Muthu, S. Singh, B. Dkhil, R. Suryanarayanan, G. Dhalenne, H. Poswal, S. Karmakar, S. M. Sharma and A. Revcolevschi, *Phys. Rev. B: Condens. Matter Mater. Phys.*, 2009, **79**, 134112.

31 S. Surblé, S. Heathman, P. Raison, D. Bouëxière, K. Popa and R. Caciuffo, *Phys. Chem. Miner.*, 2010, **37**, 761–767.

32 A. E. Ringwood and A. Major, *Phys. Earth Planet. Inter.*, 1970, **3**, 89–108.

33 F. Zhang, B. Manoun and S. Saxena, *Mater. Lett.*, 2006, **60**, 2773–2776.

34 F. Zhang, J. Wang, J. Lian, M. Lang, U. Becker and R. Ewing, *Phys. Rev. Lett.*, 2008, **100**, 045503.

35 F. Zhang, J. Lian, U. Becker, L. Wang, J. Hu, S. Saxena and R. Ewing, *Chem. Phys. Lett.*, 2007, **441**, 216–220.

36 H. Yamamura, H. Nishino, K. Kakinuma and K. Nomura, *Solid State Ionics*, 2003, **158**, 359–365.

37 F. Zhang, J. Lian, U. Becker, R. Ewing, J. Hu and S. Saxena, *Phys. Rev. B: Condens. Matter Mater. Phys.*, 2007, **76**, 214104.